11. Supplemental Figures

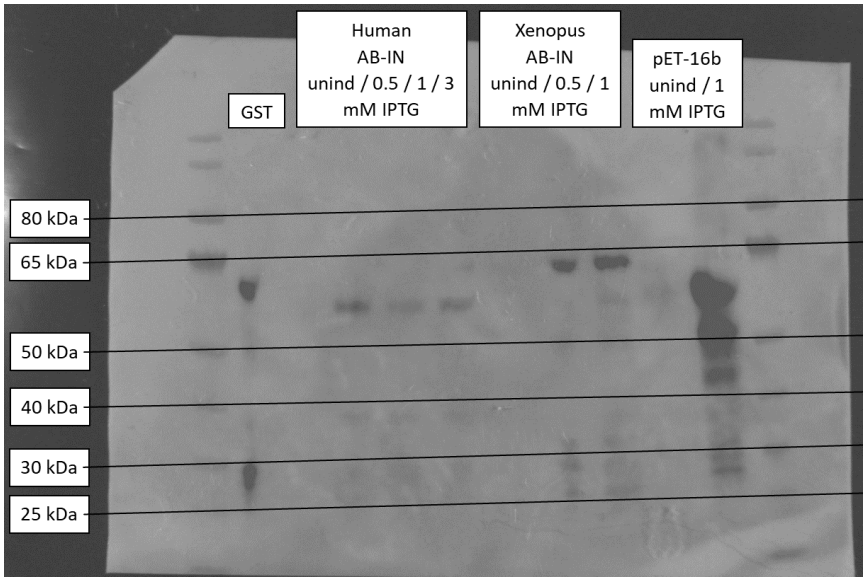

Supplemental Figure 1: Western blot of the two Aurora B kinase – INbox domain of INCENP plasmids, from human and Xenopus laevis, as well as of the positive controls, GST and a third plasmid. The rows labeled 'unind' refer to bacterial samples that were taken before induction, and were used here as negative controls. The other rows were from bacterial samples induced with various quantities of IPTG. The calculated molecular weight of the human complex is 68.7 kDa and of X. laevis, 77.6 kDa. GST has a calculated molecular weight of 25.7 kDa.

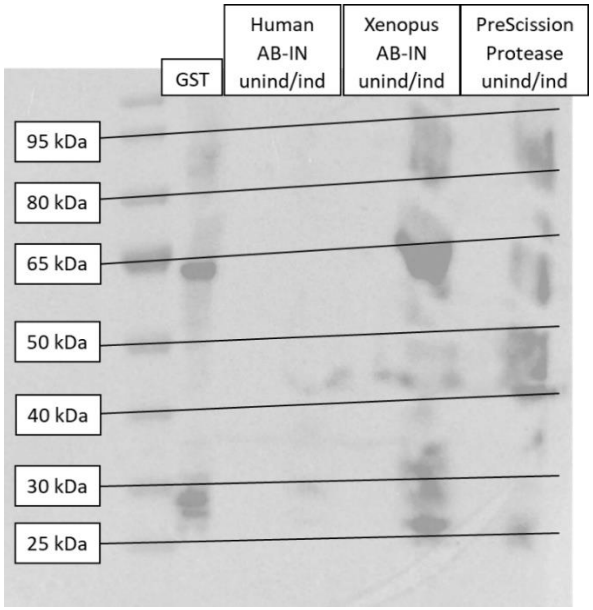

Supplemental Figure 2: Western blot of the two Aurora B kinase – INbox domain of the INCENP plasmids, of the PreScission protease, and of GST used as a positive control. The calculated molecular weight of PreScission protease is 46 kDa.

Fraction	µg/µL
1	0.58
2	2.73
3	4.55
4	6.63
5	7.19
6	5.29
Average	4.5

Supplemental Figure 3: Nanodrop A280 quantification of protein concentration in the various fractions of purified PreScission protease.

Fraction	µg/µL
1	2.8
2	10.3
3	11.4
4	10.7
5	12.7
6	10.4
Average	9.7

Supplemental Figure 4: Bradford Assay quantification of protein concentration in the various fractions of purified PreScission protease

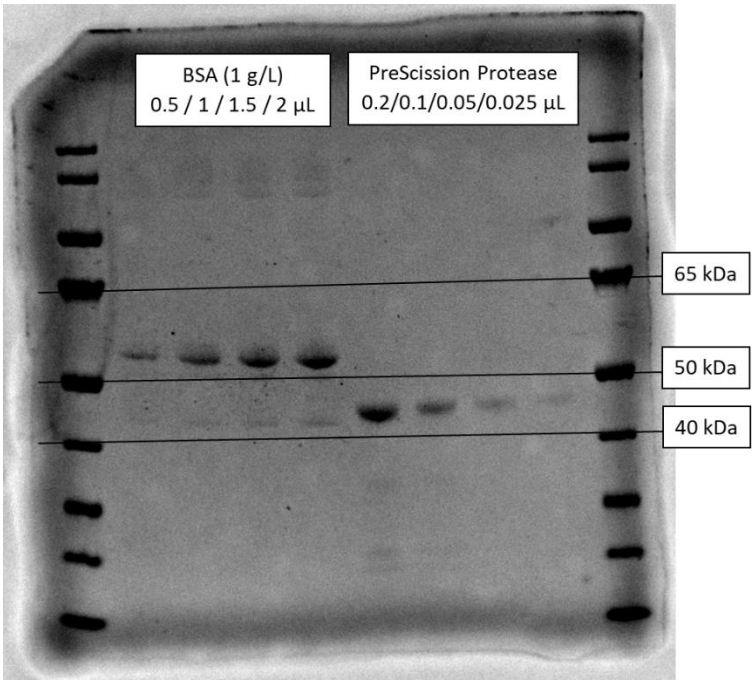

.

Supplemental Figure 5: Coomassie gel for the protein quantification of PreScission protease using BSA as calibration.

Well	BSA Weight (µg)	Pixel Intensity
1	0.5	4976
2	1	10394
3	1.5	11611
4	2	13916

Supplemental Figure 6: BSA calibration via image analysis from the Coomassie gel for protein quantification of PreScission protease.

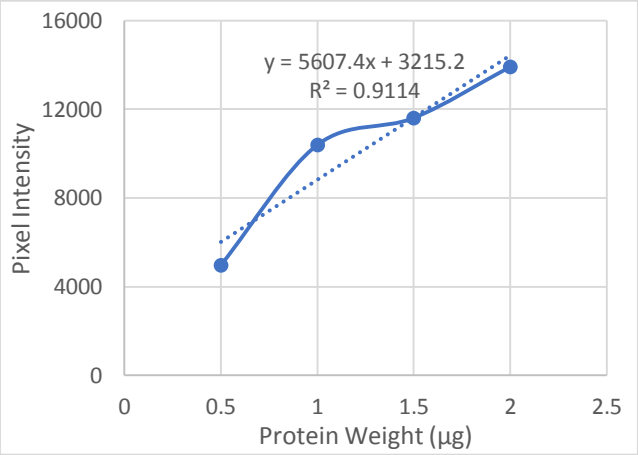

Supplemental Figure 7: BSA calibration curve using the image analysis data from the Coomassie gel for protein quantification of PreScission protease

Well	Protease Solution Volume (µL)	Pixel Intensity	Calculated Weight (µg)	Calculated Concentration (µg/µL)
5	0.2	17097	3.0	15.2
6	0.1	8241	1.5	14.7
7	0.05	3719	0.7	13.3
8	0.025	1848	0.3	13.2
			Average	15.6

Supplemental Figure 8: Quantification of PreScission protease by relating data gathered by image analysis of the Coomassie gel to the constructed BSA calibration curve.

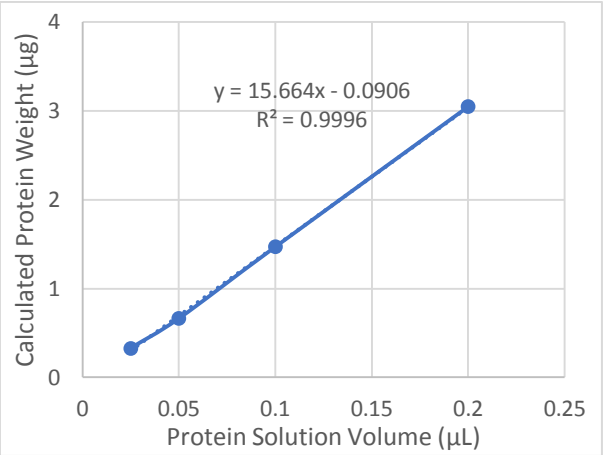

Supplemental Figure 9: PreScission protease quantification curve constructed from the various wells of the Coomassie gel.

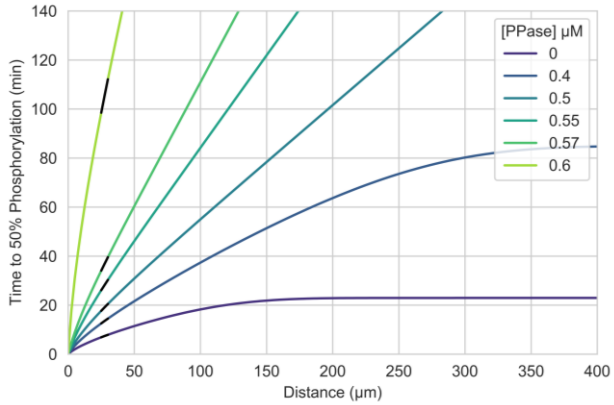

Supplemental Figure 10: Front propagation speed as determined by the time taken to reach 50% activation with respect to the high steady state, calculated for each spatial point starting from the perturbation edge for fronts with various phosphatase concentrations. Black line segments are the 3 µm linear segments reproduced in Figure 12C in the text.

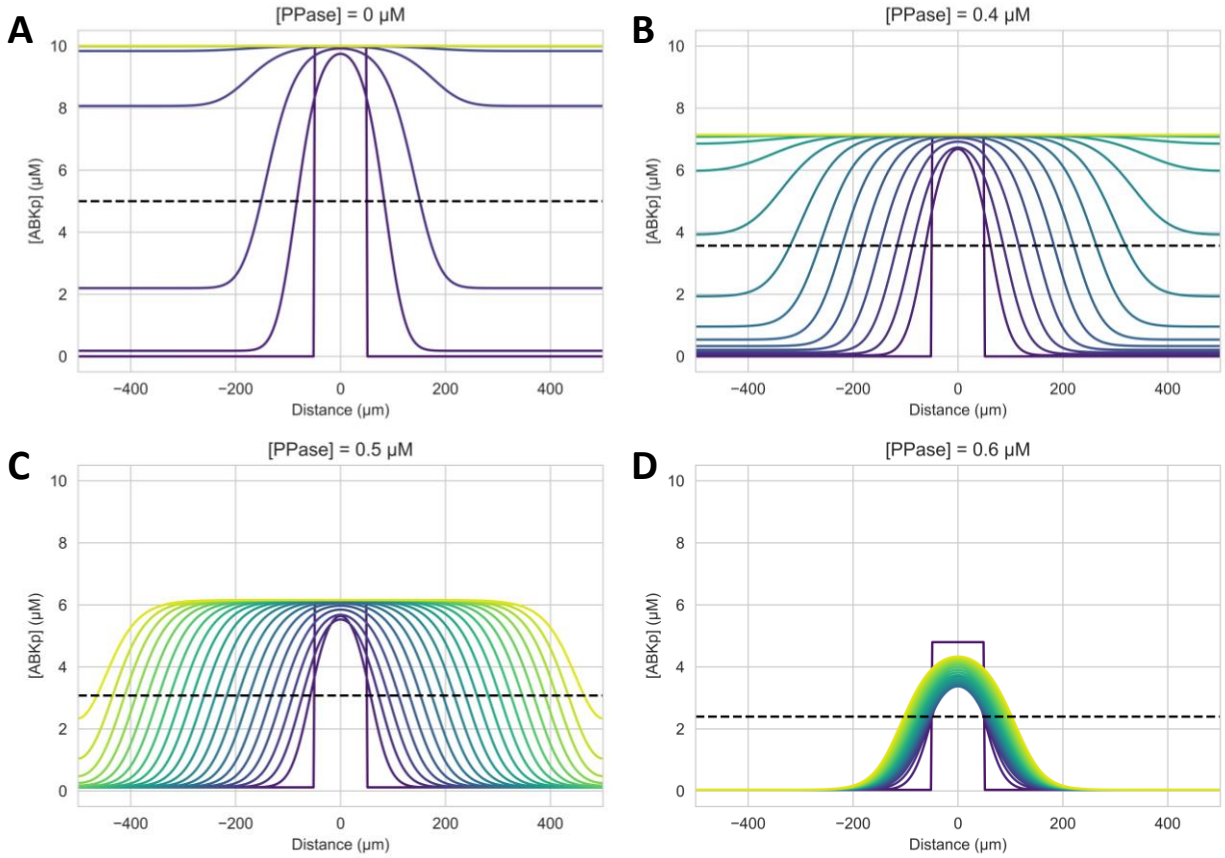

Supplemental Figure 11: Activation fronts with various phosphatase concentrations, complementing Figure 12B/C in the text. Simulations use a perturbation width of 100 μm and amplitude corresponding to the high steady state of activated Aurora B. Dashed line corresponds to 50% phosphorylation level used to calculate propagation speed.

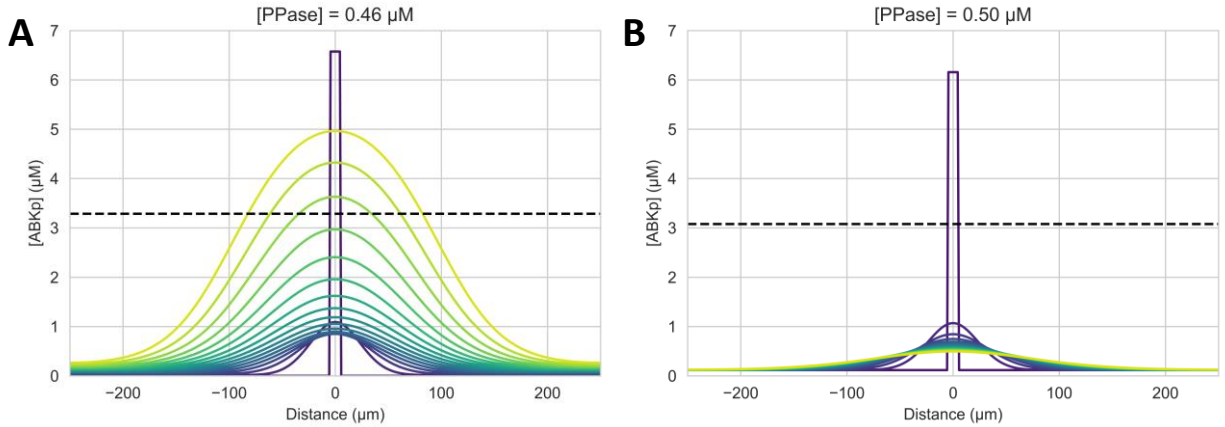

Supplemental Figure 12: Activation fronts using a perturbation width of 10 μm (A) with a phosphatase concentration lower than the bistable region and (B) with a phosphatase concentration inside the bistable region.

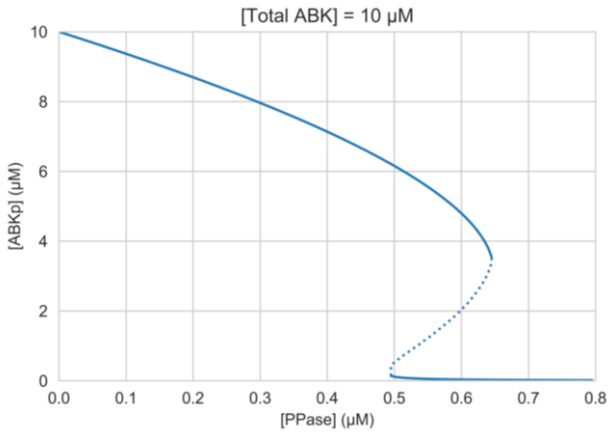

Supplemental Figure 13: Bistability curve with a total kinase concentration of 10 µm with respect to a varying phosphatase concentration, illustrating a bistable range approximately 0.5-0.65 µM phosphatase.

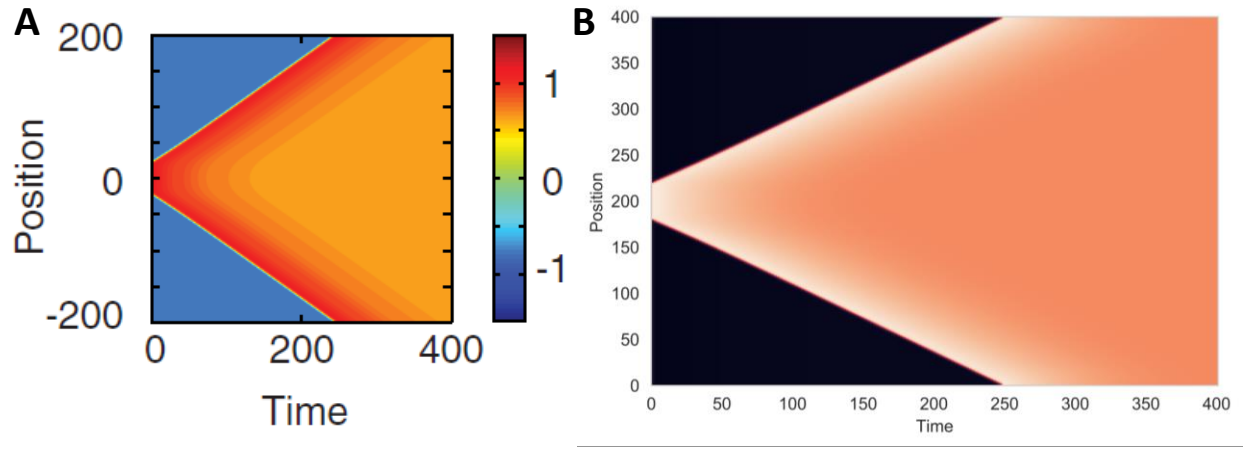

Supplemental Figure 14: Verifying Diffusion Calculation. (A) Heatmap of a bistable traveling front from coupling FitzHugh-Nagumo reaction kinetics to diffusion, reprinted from Figure 3B, Gelens, 2017. (B) Reproduced traveling front using the same kinetics, indicating the spatial derivative is calculated correctly.

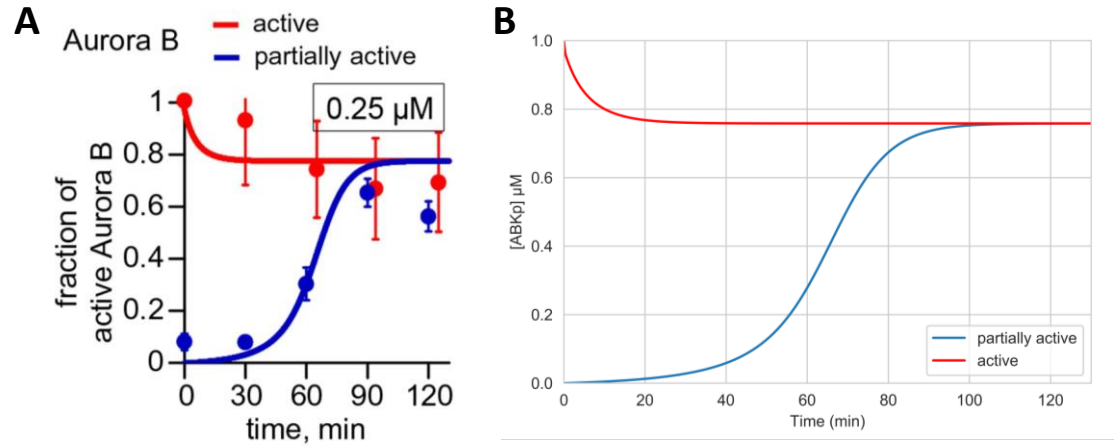

Supplemental Figure 15: Verifying Reaction Calculation. (A) Time simulation (solid lines) of reaction starting from initially active and initially inactive, labeled partially active in these plots, conditions with a phosphatase concentration of 2 µM. Reprinted from Figure 4B, Zaytsev, 2016. (B) Reproduced time simulations using the same kinetic parameters and initial conditions, indicating the reaction kinetics are calculated correctly.

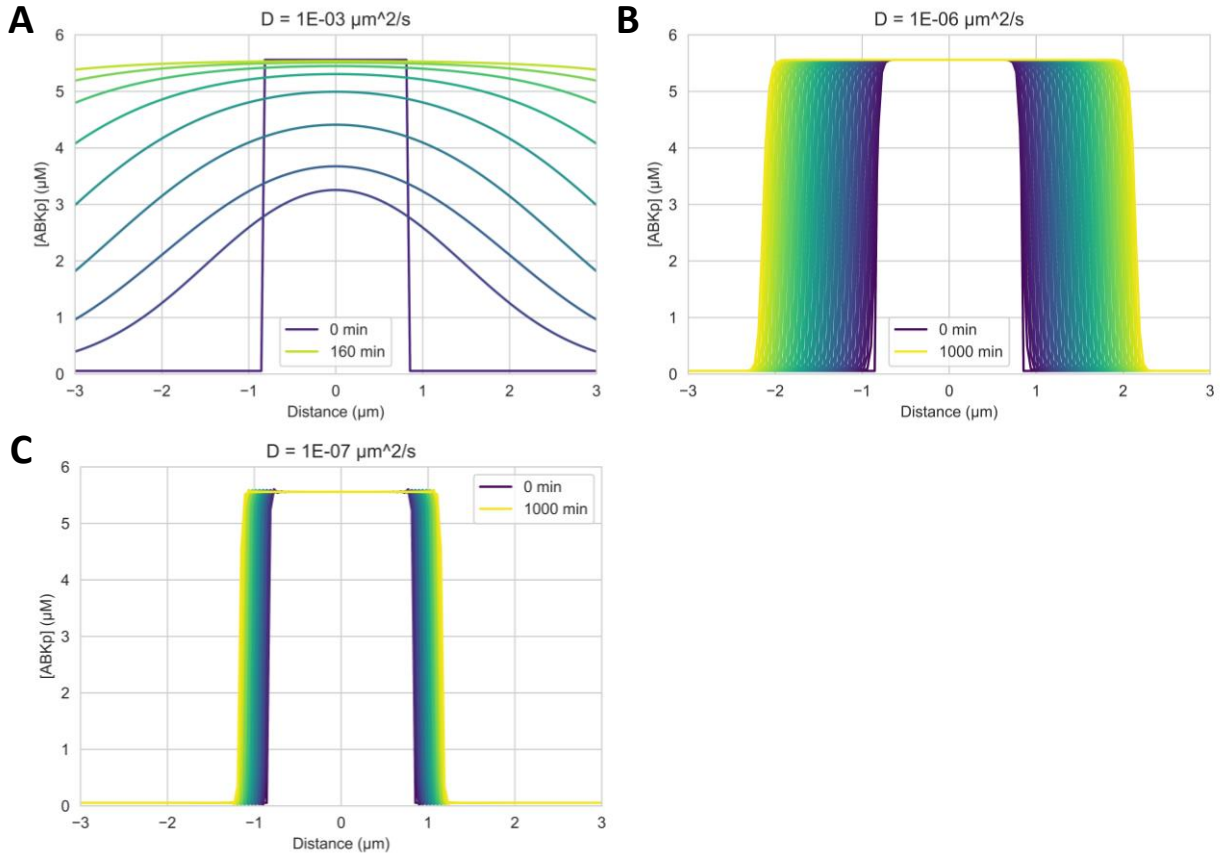

Supplemental Figure 16: Effect of Varying Diffusion Speed on Traveling Front Propagation. Intermediate diffusion speeds with respect to Figure 14 in the text. Each spatial profile is spaced 20 min from each other. Each simulation used 0.55 µM phosphatase and a spatial interval of 20 µm.

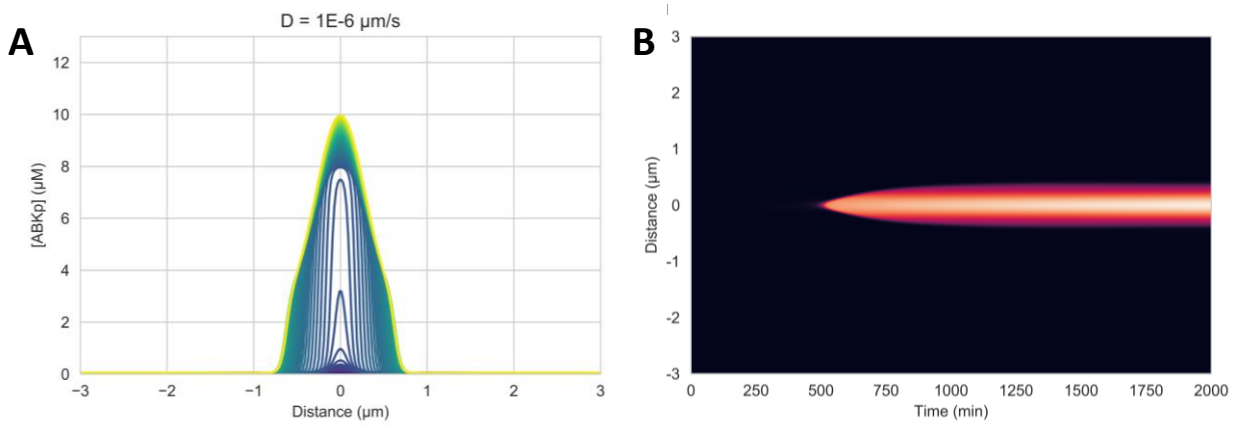

Supplemental Figure 17: Traveling front with low diffusion speed leading to wave pinning at the edge of the centromere as opposed to the traveling front propagation observed in Figure 15 in the text. (A) Spatial activation profile and (B) corresponding heatmap. Simulations use 0.55 µM phosphatase and a spatial interval of 10 µm.

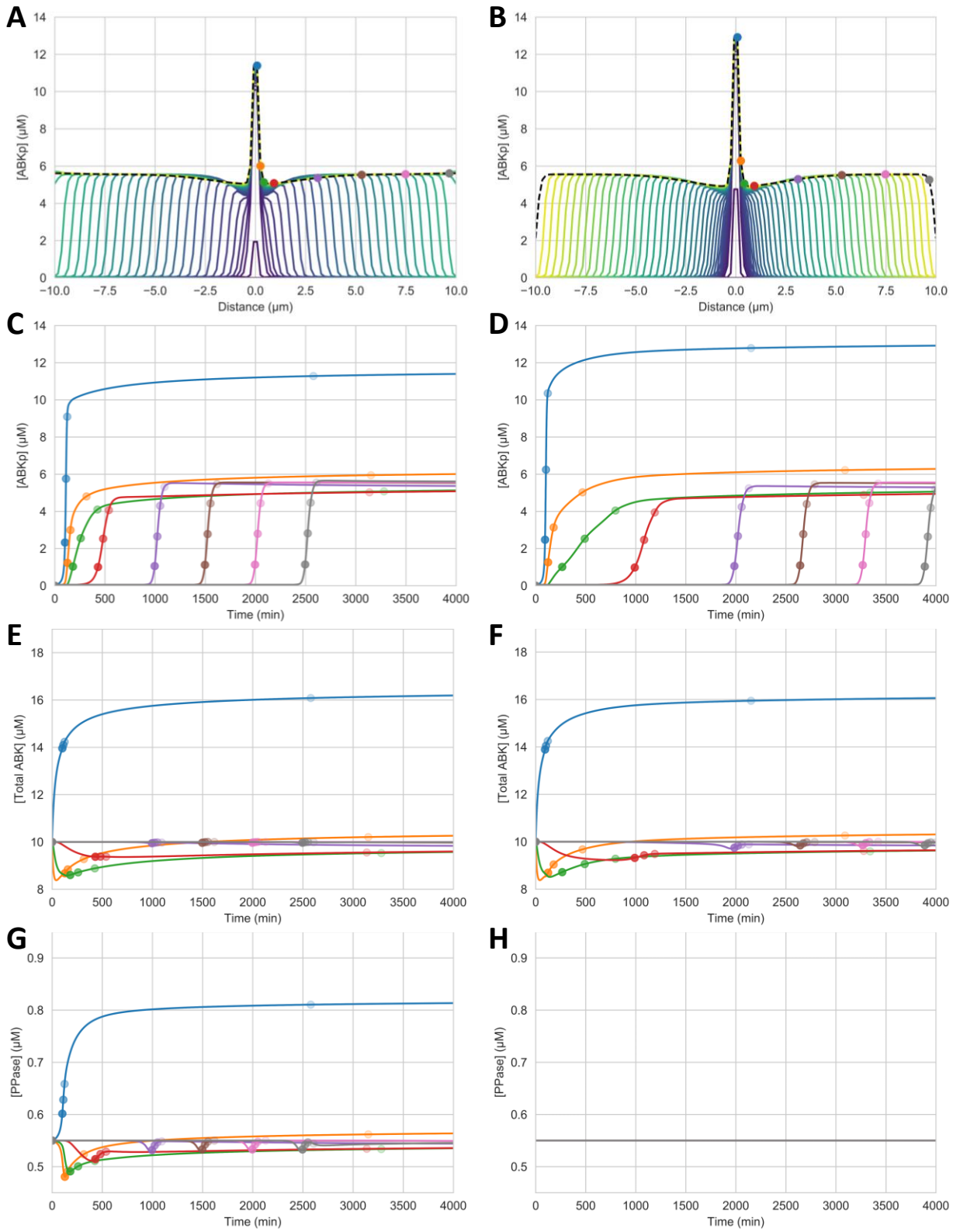

Supplemental Figure 18: (A/C/E/G) Diffusing vs. (B/D/F/H) Stationary Phosphatase. (A/B) Spatial profiles evolving in time with eight spatial discretization points to be used in dynamic analysis in the following plots: (C/D) activated kinase profiles of the discretized points, (E/F) total kinase profiles, (G/H) and phosphatase profiles. The plotted points were four time points determined by 20, 50, 80, and 99% activated kinase with respect to the high steady states.

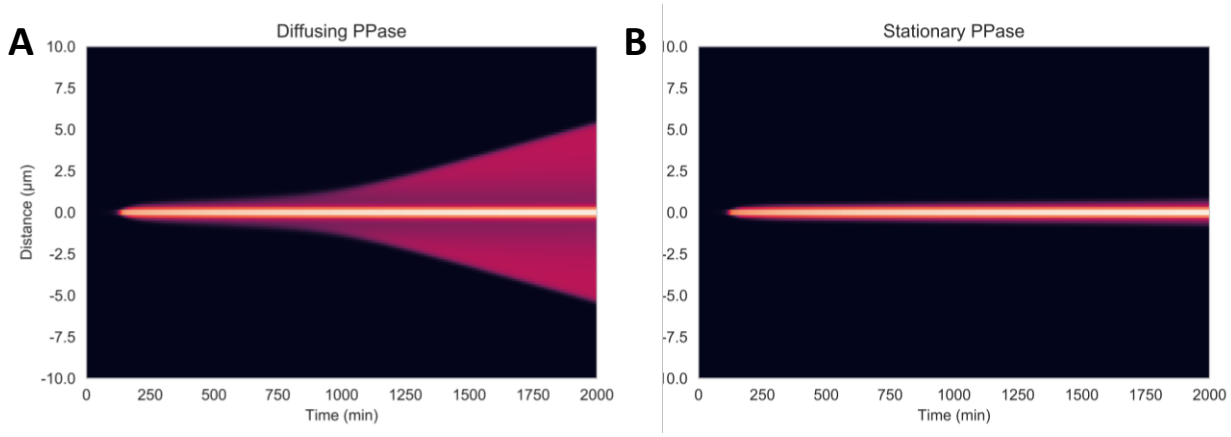

Supplemental Figure 19: Effect of Phosphatase Dynamics. Heatmaps relate with and without diffusible phosphatase. Simulations were run with the same conditions as in Figure 21. The binding site profile is wider than in Figure 22, showing a pinned front when phosphatase is fixed.

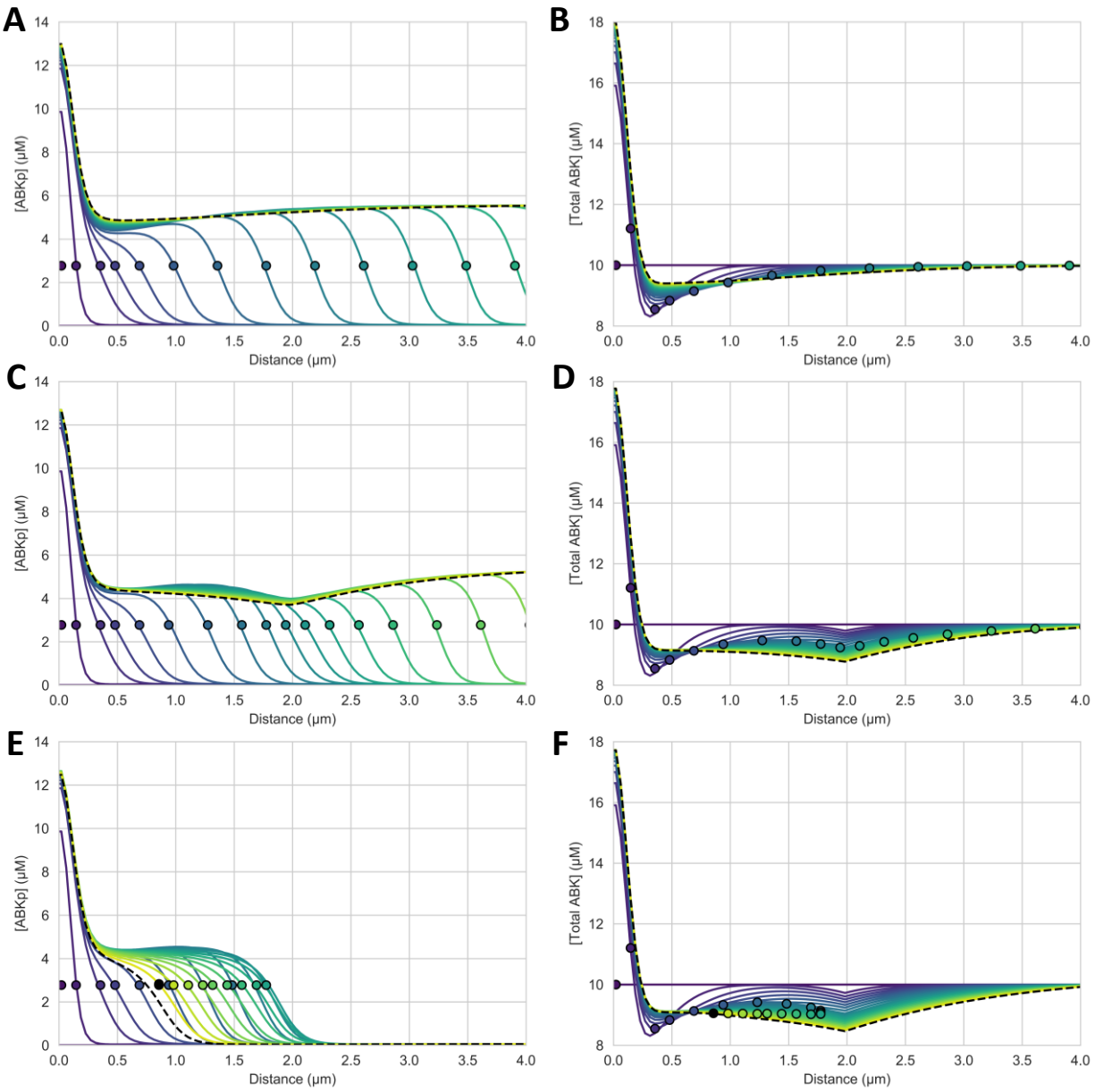

Supplemental Figure 20: Progress of traveling wave along second order kinase profiles. (A/C/E) Spatial activation profiles with points tied to the front boundary at 50% activation and (B/D/F) related kinase profiles. Binding site profiles with (A/B) no ramp, (C/D) intermediate slope, and (E/F) high slope. Figure corresponds to Figure 23 in the text.

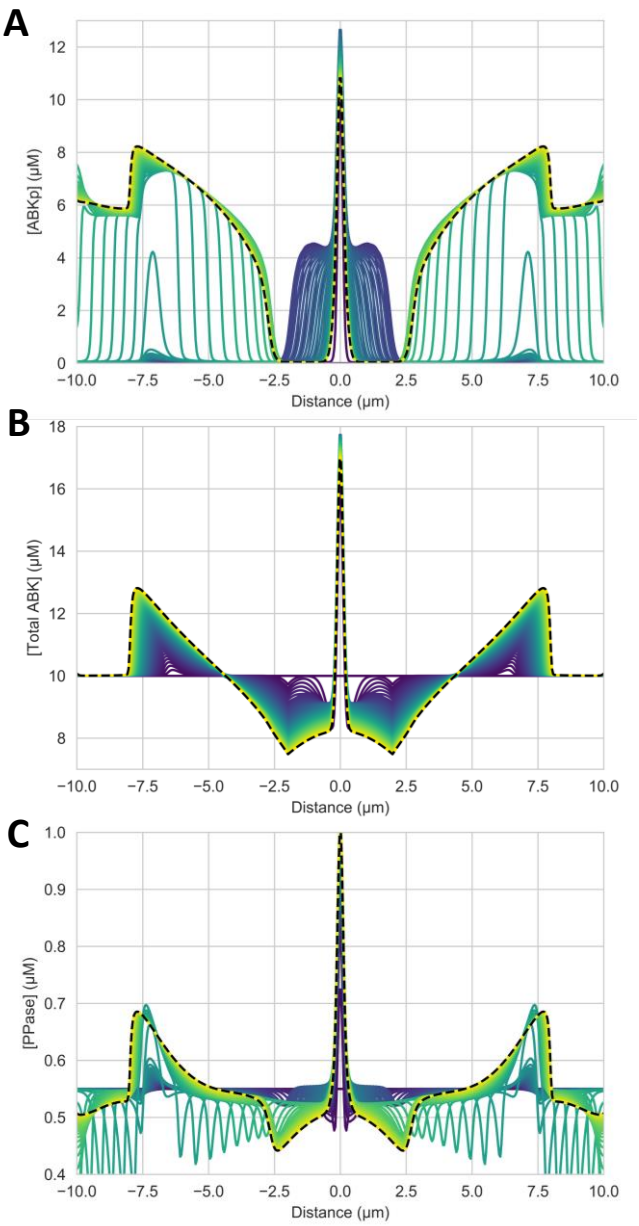

Supplemental Figure 21: Non-centromeric autoactivation in systems with high binding site ramps. Spatial profiles of (A) active kinase, (B) total kinase, and (C) phosphatase. Figure corresponds to Figure 24 in the text.

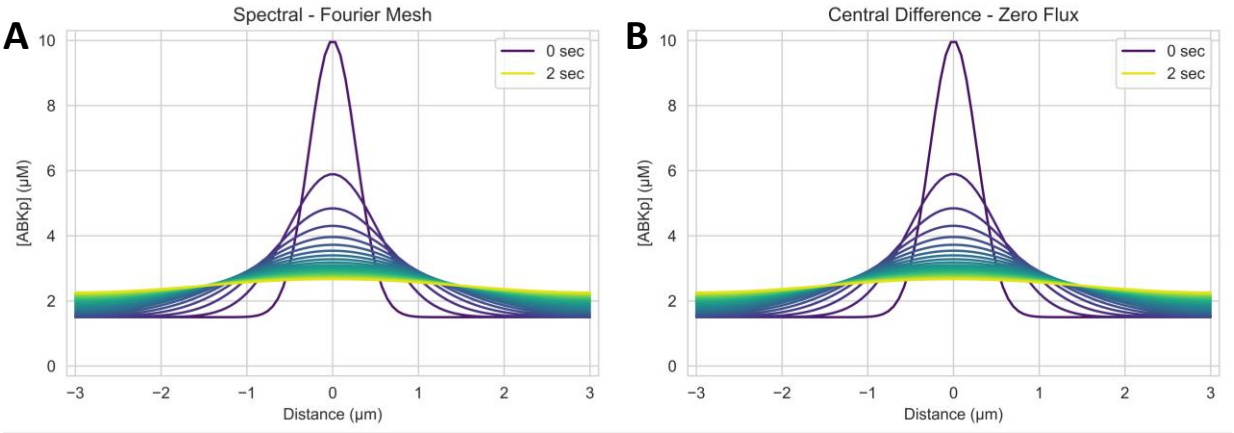

Supplemental Figure 22: Different methods to solve the space derivative. (A) Spectral method via Fourier mesh with implicit periodic boundary conditions (B) and central difference with zero flux boundary conditions.